# Carbon nanotubes hybridized graphene oxide composite for efficient capture of cationic dye from aqueous solution

Eman M. Saad[a],*, Hassan M.A. Hassan[a,b],*, E.A. El-Sharkawy[a], Mohamed S. Gaber[a]

[a]*Department of Chemistry, Faculty of Science, Suez University, Suez, Egypt, emails: emmsaad@yahoo.com (E.M. Saad),*
*h.hassan@suezuniv.edu.eg (H.M.A. Hassan), easharkawy63@yahoo.com (E.A. El-Sharkawy), chemist.msg@gmail.com (M.S. Gaber)*
[b]*Department of Chemistry, College of Science, Jouf University, P.O. Box: 2014, Sakaka, Saudi Arabia*

## ABSTRACT

A carbon architecture composite was made from multiwalled carbon nanotubes (MWCNTs) with graphene oxide (GO) (MWCNTs-10/GO and MWCNTs-COOH-10/GO) and nominated as an adsorbent for methylene blue (MB) removal from contaminated water to further improve the organic pollutants capturing effectiveness. Scanning electron microscopy, energy-dispersive X-ray spectroscopy, transmission electron microscopy, Raman, Fourier transform infrared spectroscopy and X-ray diffraction spectra were used to perform the composition and textural features of the obtained composites. Several parameters were applied to reach the maximum adsorption capacity, which is pH 8.5 with contact time 60 min and 25°C, using 10 mg of composite. The removal capacities of MWCNTs/GO and MWCNTs-COOH/GO composites for removal of MB are found to be 705.4 and 850.1 mg g$^{-1}$, respectively. The adsorption rate of dye onto composites well-stated by the pseudo-second-order model. Spontaneous and exothermic adsorption processes were verified by the thermodynamic parameters ($\Delta H°$, $\Delta S°$, and $\Delta G°$). Sequential adsorption–desorption processes showed that MWCNTs-10/GO and MWCNTs-COOH-10/GO retain their adsorption efficiency over four cycles. Thus, the composites carbon architecture was regarded as achievable and auspicious candidates for removing MB from contaminated water with high capacities and recycling.

*Keywords:* Graphene oxide; Carbon nanotubes; MB adsorption; Removal, Carbon composites

## 1. Introduction

Aromatic dyes are chemicals widely adopted for paper, plastics, pulp mill, printing ink, textile, leather, nutrition, and cosmetics manufacturing. However, the main drawbacks associated with the dyes, for instance, the easily released into the aqueous environment due to their great dissolution in water. The complex structures and xenobiotic characteristics make dyes non-biodegradable, harmful and present some major environmental, safety, and ecological issues [1–4]. Thereby, wastewater containing excessive dyes must be addressed robustly prior to discharging into natural water. Currently, several approaches have been adopted for the capturing of dyes from the aquatic medium, such as adsorption [5–7], chemical coagulation [8], membrane separation [9], photocatalytic degradation [10,11] and biological treatment [12]. Most of these technologies are suffering from significant disadvantages (harsh to handle and not economic). To beat such drawbacks, adsorption technology is being suggested as a promising economic consideration; that is, with high accessibility, low cost, high performance, and no harmful by-product. Since seeking adequate, environmentally friend efficient cost materials sorbents are still of interest, commercial sorbents, such as rice hush, bamboo-based active carbon, coir pith carbon, activated clay and activated

---

* Corresponding authors.

desert plant were extensively investigated for the removal of dyes from aqueous media [13–17]. The adsorption depends on the high surface area of the sorbents, adequate pore size, and high chemical stability for long period operations.

With respect to nanotechnology, novel carbonaceous sorbents such as carbon nanotubes [18] and graphene [19] have received interest owing to their high adsorption capacity, low density, stability, and appropriateness big scale fabrication as compared to the convention sorbents.

Graphene oxide (GO) is one of the most outstanding progressing carbon-based materials possessing two-dimensional honeycomb sp$^2$-carbon lattice, unique electronic, the high surface area around to 2,630 m$^2$ g$^{-1}$ and superior chemical stability [20,21]. GO, an oxidized derivative of graphene possesses some amazing characteristics such as good mechanical strength, hydrophilicity and easy dispersion in aqueous solutions due to its hydroxy, epoxy and carboxylic moieties. Moreover, GO can be easily fabricated using exfoliation of the natural graphite chemically [22,23]. Therefore, graphene and GO derivative is of great interest as an alternative promising sorbents for the adsorption of various pollutants from aqueous medium. Moreover, carbon nanotubes (CNTs) are popular materials for various applications such as separation, sensors, adsorption, catalysis, biomedicine and electronic apparatus [24–29]. CNTs exhibit superior adsorption capacity for capturing different types of inorganic and organic contaminants from aquatic medium [30]. However, free CNTs are scarcely utilized for sorption owing to van der Waals forces of whole carbon atoms in graphene nanosheets. In contrast, functionalized CNTs are good adsorbents for the capturing of metal ions due to the grafting which enhance the dispersion and the adsorption capacity of metal ions via the chemical interaction, which would be more selective than the free ones, owing to the introduction of carboxyl moieties on the carbon nanotubes surface [31–38].

In this study, we explore the synergistic impacts between 2-dimensional GO and 1-dimensional multiwall carbon nanotubes decorated with –COOH moieties for high-performance organic contaminants removal. A facile one-step chemical approach was proposed for the fabrication of multiwalled carbon nanotubes (MWCNTs)/GO composite. To emphasize the adsorption performance of the fabricated composites, methylene blue (MB) as a model organic contaminant dye was selected. The MB adsorption kinetic and isotherm on the MWCNTs/GO composite were investigated. This study suggested the utility of these carbon-based materials as an active adsorbent for remediation of the environment.

## 2. Experimental section

### 2.1. Fabrication methods

#### 2.1.1. Graphite oxide fabrication

GO was fabricated from graphite powder (Fisher Scientific, 99%, USA) by modifying the Hummers method [39,40]. For refinement, the collected cake was separated and the solids rinsed with HCl (5%) and deionized water for many times. The final product was vacuum dried at room temperature overnight.

#### 2.1.2. Functionalization of MWCNTs

MWCNTs-COOH were obtained via oxidation process. 500 mg of MWCNTs was added to 250 ml 3 M HNO$_3$ and the mixture well dispersed by sonication for about 30 min using ultrasonic (35 kHz, 70 W). The mixture was then stirred and refluxed at 110°C for 48 h. The powder was filtrated by centrifugation, rinsed several times with water and dried under vacuum 110°C for 12 h [41].

#### 2.1.3. MWCNTs/GO and MWCNTs-COOH/GO nanocomposite fabrication

MWCNTs/GO and MWCNTs-COOH/GO nanocomposites with various carbon nanotubes concentration were fabricated by the reported simple one-step method [42,43]. Typically, GO was sonicated for 10 min. MWCNTs or MWCNTs-COOH powder with a ratio of 5, 10, 15, and 20 (w/w) were then added to the suspension while sonicating [44]. The fabricated composite was further sonicated for 40 min for complete homogeneity. The final product was separated, rinsed several times with water followed by drying at 110°C (to prevent the oxidation of the nanotubes that take place at high temperatures). The symbolic designation of the prepared composites is donated as MWCNTs-5/GO, MWCNTs-10/GO, MWCNTs-15/GO, and MWCNTs-20/GO or MWCNTs-COOH-5/GO, MWCNTs-COOH-10/GO, MWCNTs-COOH-15/GO, and MWCNTs-COOH-20/GO, respectively.

### 2.2. Characterization

Powder X-ray diffraction (XRD) was investigated using Siemens D5000 X-ray powder diffractometer (Germany), operating with monochromatized CuK$\alpha$ radiation (40 mA and 45 kV). The Raman spectra were collected on Enwave Optronics ProRaman-L spectrometer via an excitation wavelength of 532 nm laser. A Shimadzu IRTracer-100 Fourier transforms infrared spectrophotometer (Japan) was applied to monitor Fourier transform infrared spectroscopy (FTIR) spectrum. High-resolution transmission electron microscopy (HRTEM) images were carried out using a JEOL 2011 electron microscope (Japan) operated at 200 kV. The morphology of the composite materials was investigated via a Zeiss scanning electron microscopy, (Germany) (SEM) Ultra 60 field emission scanning electron microscopy (FESEM). The concentrations of dye were determined using a UV–visible spectrophotometer (A Shimadzu-1601PC UV-Visible automatic recording spectrophotometer, Japan).

### 2.3. Adsorption assessment

The adsorption of MB from aquatic solution onto the fabricated materials was carried out in batch experiments and proceed in triplicate. Typically, a solution of 50 mL MB having initial concentrations (50 mg L$^{-1}$) was added to 10 mg of the sorbent at the pH range of 2–11.5 under constant shaking time of 120 min. and constant temperature. A series of experiments were conducted at different time intervals (15–180 min) at constant dye concentration (500 mg L$^{-1}$), pH, dose and temperature. For the isotherm

study, the concentration of dye varies from 50–700 mg L$^{-1}$ while the other parameters were constant. The removal efficiency (%), the quantity of MB dye removed per unit mass of the composite at equilibrium and time *t* were calculated by Eqs. (1)–(3):

$$\text{Dye removal}, \% = \frac{(C_0 - C_e)}{C_0} \times 100 \qquad (1)$$

$$Q_e \left(\text{mg g}^{-1}\right) = \frac{(C_0 - C_e)V_L}{W_g} \qquad (2)$$

$$Q_t \left(\text{mg g}^{-1}\right) = \frac{(C_0 - C_e)V_L}{W_g} \qquad (3)$$

where $C_0$ mg L$^{-1}$, $C_e$ mg L$^{-1}$, $Q_e$ and $Q_t$ the initial concentration, concentration of dye at the equilibrium, adsorption capability at equilibrium and time (*t*), respectively, *m*(g) is the sorbent mass and *V*(L) is the dye volume.

### 2.4. Desorption experiments

The evaluation of the reusability of the MWCNTs-10/GO and MWCNTs-COOH-10/GO adsorbents were carried out by using 10 mg dosage of adsorbent, which added to 50 mL of 50 mg L$^{-1}$ dye solutions for 60 min, and the adsorbent was isolated from the solution. The desorption and recycling of the adsorbent were accomplished by soaking the adsorbent loaded with dye in 50 mL of a 0.1 M NaCl/HCl mixture for 6 h at ambient temperature and then rinsed it with water until neutral for the next adsorption. The recycled adsorbents were applied for subsequent adsorption research.

## 3. Result and discussion

### 3.1. Characterization of sorbents

Fig. 1a shows the XRD profiles of the bare graphite powder and GO. Pristine graphite powder depicts the distinct sharp diffraction peak centered at 2θ 26.72°, related to d-spacing of 3.32 Å. GO was fabricated by graphite powder oxidation process; that is, grafting of hydroxy and epoxy moieties among the carbon sheets along with carboxylic moieties present on the terminal and lateral sheet sides [40], which leads to the reduction of van der Waals forces among the graphite sheets in the exfoliated GO. The XRD pattern of the exfoliated GO shows a broad peak around 2θ 8.9° owing to the existence of oxygen function moieties which leads to increasing the distance between the carbon sheets as compared in the pristine graphite. The XRD (Fig. 1b) of pristine MWCNTs, exhibit four peaks centered at 2θ 14.9°, 25.3°, 42.6°, and 44.2°, attributing to the hexagonal structure. Moreover, the XRD diffraction patterns of the fabricated composites depicted a wide (002) peak at 2θ = 25.3°, which was much greater than that of pure GO. This result reveals a decline in the *d*-spacing of GO in the composite, stemming from the strong interaction between graphene and MWCNTs and change in the layer space in the presence of MWCNTs.

Figs. 2 and 3 display the FTIR and Raman spectra of both bare MWCNTs and MWCNTs-COOH, respectively. Pristine MWCNTs showed a wide absorption band at 3,428 cm$^{-1}$ owing to ν(OH) of hydroxy and carboxylic groups. This band became more obvious in the functionalized MWCNTs-COOH sample. The band close 2,369 cm$^{-1}$ is assigned to ν(OH) stretch of robustly H-bonded −COOH moieties. The appearance of carboxylic moieties joined to the surface of MWCNTs could be attributed to partial oxidation during the fabrication. Raman spectra of all composite materials display two eminent peaks at 1,352 and 1,580 cm$^{-1}$ assigned to the D and G bands (sp$^3$ and sp$^2$-hybridized C, respectively) [44]. The G band exhibits a blue shift (potential interaction between GO and CNTs). Additionally, the D/G band ratio was applied to assess the goodness of the graphitic skeleton since the D/G ratio approaches zero for extremely ordered pyrolytic graphite [44]. The intensity ratios of the D band and the G-band ($I_D/I_G$) of MWCNTs, MWCNTs-10/GO, and MWCNTs-COOH-10/GO were 0.945, 1.002, and 1.023 respectively, indicating that the sp$^3$-hybridized carbon atoms in the functionalized
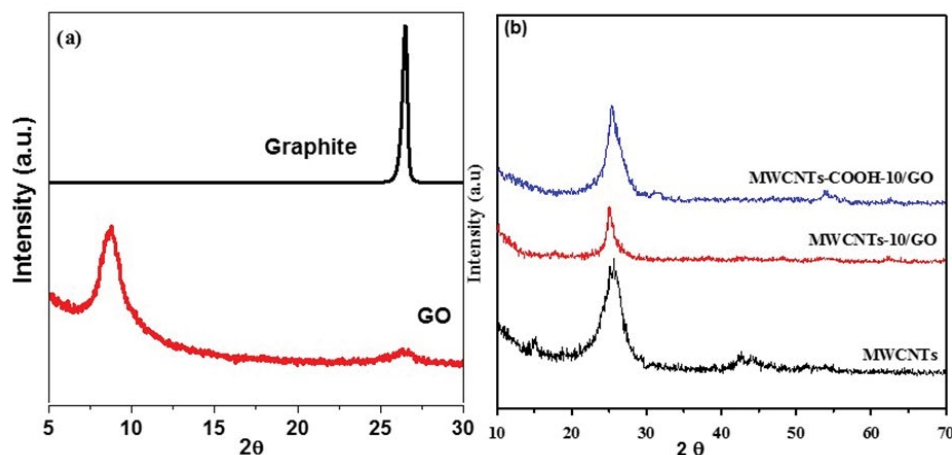


Fig. 1. Small-angle (a) of GO and (b) wide-angle patterns of pristine MWCNTs, MWCNTs-10/GO and MWCNTs-COOH-10/GO composite.
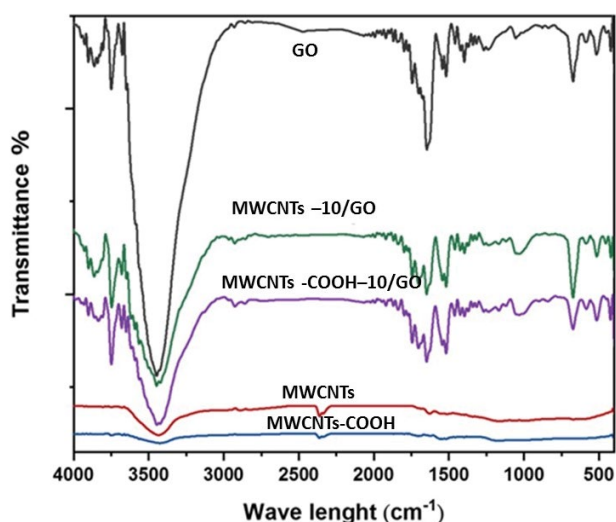
Fig. 2. FTIR spectra of GO, MWNTs, MWCNTs-COOH, MWCNTs-10/GO, and MWCNTs-COOH-10/GO samples.

composite MWCNTs-COOH-10/GO are greater than that of MWCNTs-10/GO; that is, response to the formation of more oxygen-containing function group in MWCNTs-COOH-10/GO. Prior to the functionalization, the obtained sharp 2D band of MWCNTs was observed at 2,689 cm$^{-1}$ (attributed to few-layer graphene sheets). The 2D shape after functionalization became weak significantly, due to the stacking of sheets in the composite. The MWCNTs-COOH spectrum displays identical spectrum pristine MWCNTs. Further bands were observed at 1,504 and 1,712 cm$^{-1}$ can be ascribed to v(COOH) moieties, which were created due to the acid treatment process of carbon atoms over MWCNTs surface.

SEM image of GO (Fig. 4a) displayed the layered structures with bent, thin and unruffled properties, while that of the pristine MWCNTs (Fig. 4b) showed smooth and

intertwined network structure, producing a huge number of mesopores. Upon comparing GO and MWCNTs with the MWCNTs/GO composite (Figs. 4c and d), a hierarchical structure was observed as a result of the interaction of 1-D MWCNTs into 2-D graphene. Energy-dispersive X-ray spectroscopy (EDX) pattern of GO and MWCNTs-COOH/GO loaded with MB dye shown in Figs. 4e and 4f. The EDX results exhibit the presence of C, O, and Cl, N, and S of GO and MWCNTs-COOH pattern, respectively, indicating the adsorption of MB on the composite [45]. Transmission electron microscopy (TEM) was further applied to estimate the morphology of the composite materials. GO (Fig. 5a) showed crimpy and slightly bent sheets with a side dimension up to little micrometers. The bare MWCNTs (Fig. 5b) showed a smooth and twisted web structure, producing a huge number of mesopores. The images of MWCNTs/GO and MWCNTs-COOH/GO hybrid materials (Figs. 5c and d) showed typical TEM image of MWCNTs/GO composite which revealed that there are amount of MWCNTs with lengths of various micrometers were well distributed and closely attached on the GO surface which was ultra-large, flat and complete. There are clusters of MWCNTs combined above the large GO sheets and integrate into the gaps among different GO layers in the wrinkled and curled edges. MWCNTs were decumbent and interlocking in the transverse direction between GO sheets to enhance the stability and separating sheets in linear trend to hinder stacking. Moreover, the carbon structure with a tubular texture was remaining unchanged after functionalization and conjugation as a composite (Fig. 5d).

### 3.2. Adsorption assessment

Influence of different adsorption conditions such as contact time, pH, dose and initial concentration of MB were estimated for optimization of the removal conditions using MWCNTs-10/GO and MWCNTs-COOH-10/GO as a model sorbent.
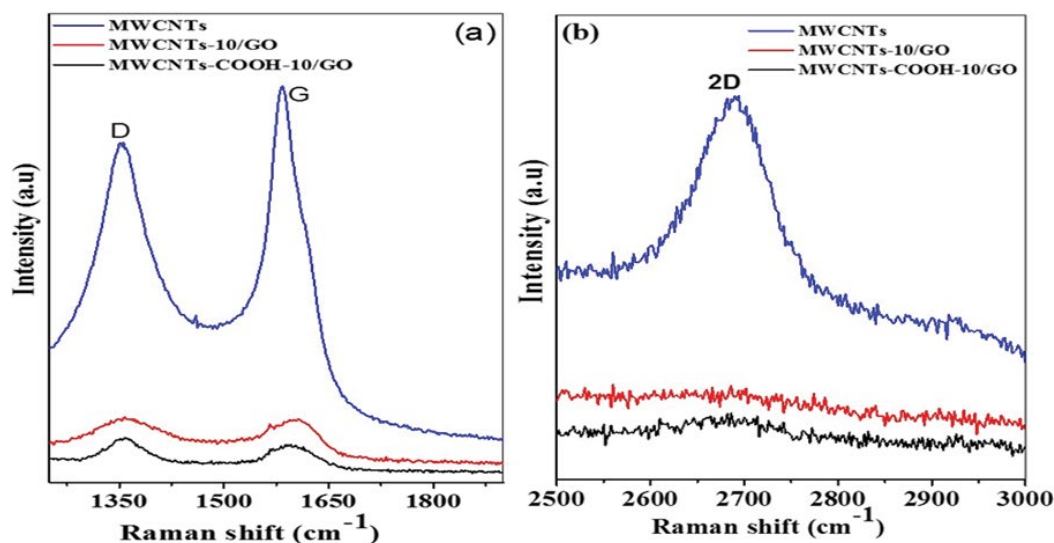


Fig. 3. (a) Raman spectra D and G band and (b) 2D band of pristine MWCNTs, MWCNTs-10/GO and MWCNTs-COOH-10/GO composites.
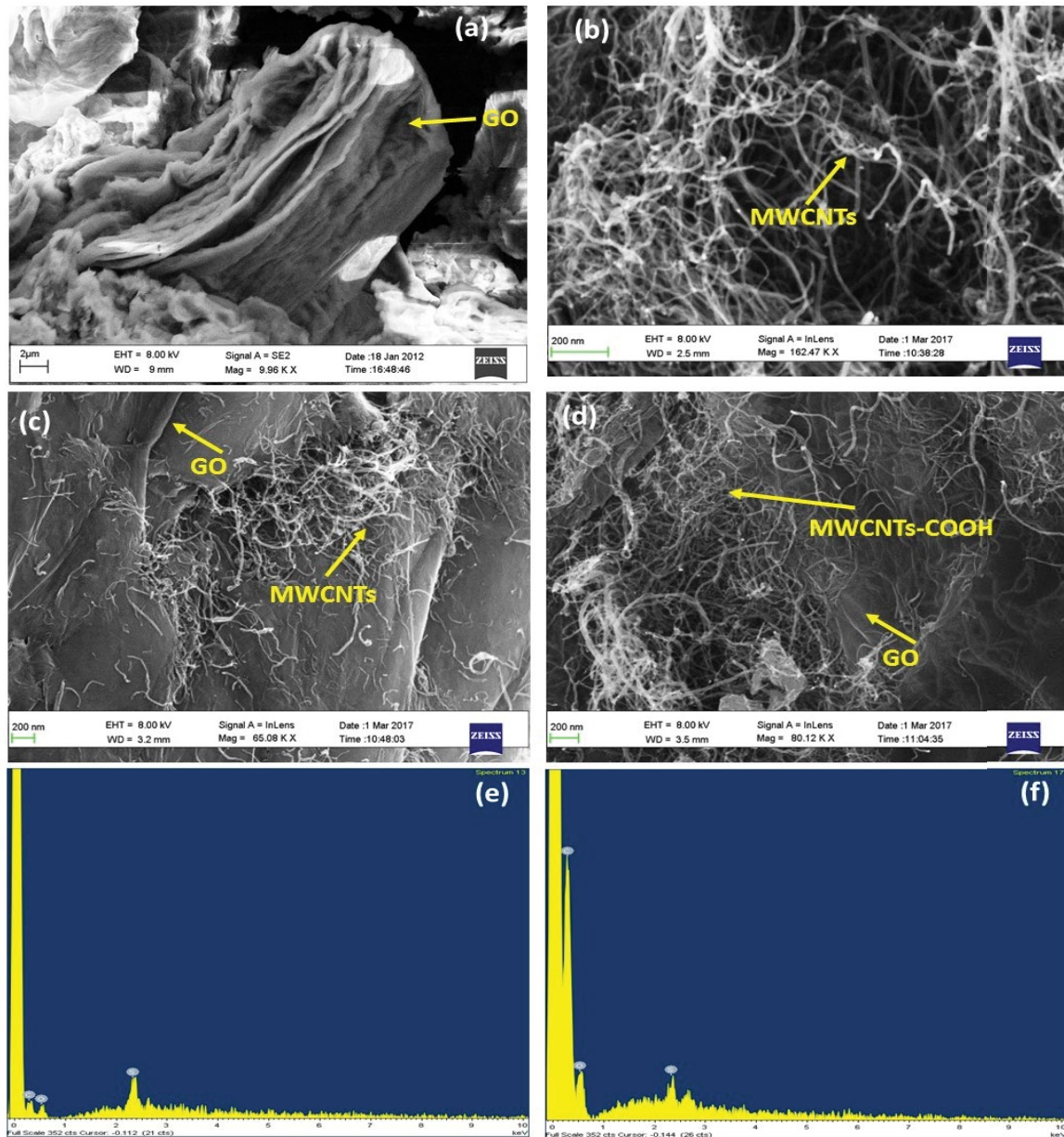
Fig. 4. FESEM images of (a) pristine GO, (b) pristine MWCNTs, (c) MWCNTs-10/GO, (d) MWCNTs-COOH-10/GO, (e) EDX of GO and (f) EDX of MWCNTs-COOH/GO loaded with MB.

### 3.2.1. Influence of MWCNTs ratio

Table 1 displays the influence of the MWCNTs ratio on the elimination efficiency of MB dye. The removal percent increases with increasing the MWCNTs at 10% by mass and decreases at 20%. Therefore, the ratio of 10% was found to be suitable for the removal processes.

### 3.2.2. Influence of pH

The solution pH is a vital parameter affecting the removal capacity in the removal process. The impact of the initial pH value on the MB removal is displayed in Fig. 6a. It is worth noting that the maximum adsorption performance of MB at pH 8 and higher was attained. At low pH, the surface of the sorbents MWCNTs-10/GO and MWCNTs-COOH-10/GO were highly positively charged (due to the protonation of COOH, OH moieties). Furthermore, a considerable coulombic repulsion produced between the composite surface and the cationic dye solution leading to minimum adsorption. However, as the pH of the solution increases the composite surface acquired a negative charge which could be attributed to the deprotonation of the surface functional moieties (COO⁻, O⁻) over the adsorbent's surfaces with $pK_{as}$ = 4.76 and 8.0 values for –COOH and –OH groups, respectively (Fig. 6b) [46–48]. High negative charges of the adsorbents
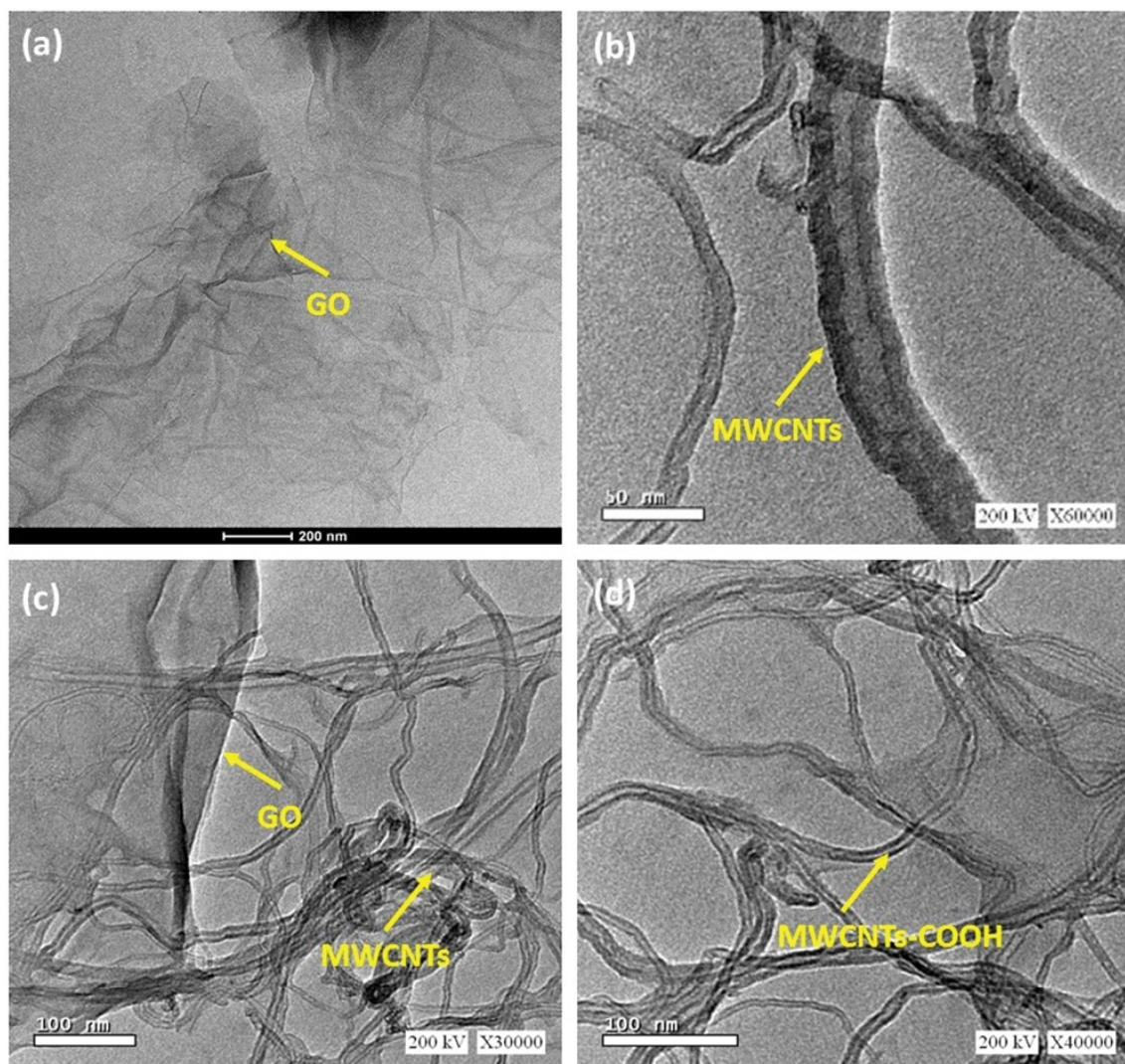
Fig. 5. HRTEM images of (a) pristine GO, (b) pristine MWCNTs, (c) MWCNTs-10/GO, and (d) MWCNTs-COOH-10/GO composites.

Table 1
Influence of MWCNTs ratio on the removal % of MB at optimum parameters

| Ratio %(wt./wt.) | Removal, % | |
| --- | --- | --- |
| | MWCNTs-10/GO | MWCNTs-COOH-10/GO |
| 5 | 65.2 | 78.7 |
| 10 | 97.8 | 99.37 |
| 15 | 95.35 | 97.45 |
| 20 | 83.5 | 88.75 |

could enhance the coulombic attraction resulting in an improvement in the removal capacity of MB. Additionally, at higher pHs, the liberated H$^+$ ions could be decreased through the neutralization process, which furtherly assists the adsorption. The impact of pH on the removal of MB was more explicit in the case of functionalized MWCNTs-COOH-10/GO than the non-functionalized MWCNTs-10/GO,

the adsorption capacities were 246.5 and 224.1 mg g$^{-1}$, respectively, at pH 8.5. Thus, pH 8.5 was adopted in the subsequent experiments.

### 3.2.3. Influence of contact time

The impact of contact time on the adsorption efficacy of MB was measured at pH 8.5 using adsorbent dose (10 mg). The highest adsorption capacity of MB was obtained at equilibrium time 60 min for both MWCNTs-10/GO and MWCNTs-COOH-10/GO adsorbents (Fig. 7). Raising the adsorbed time to 180 min depicted that the MB adsorption was not considerably altered as compared with those obtained at 60 min, as increasing the time lead to accumulation of the dye molecules, which hinders the diffusion of aggregated dye molecules into the adsorbents.

### 3.2.4. Effect of adsorbent dose

The effect of MWCNTs-10/GO and MWCNTs-COOH-10/GO adsorbents amount on MB removal was performed by
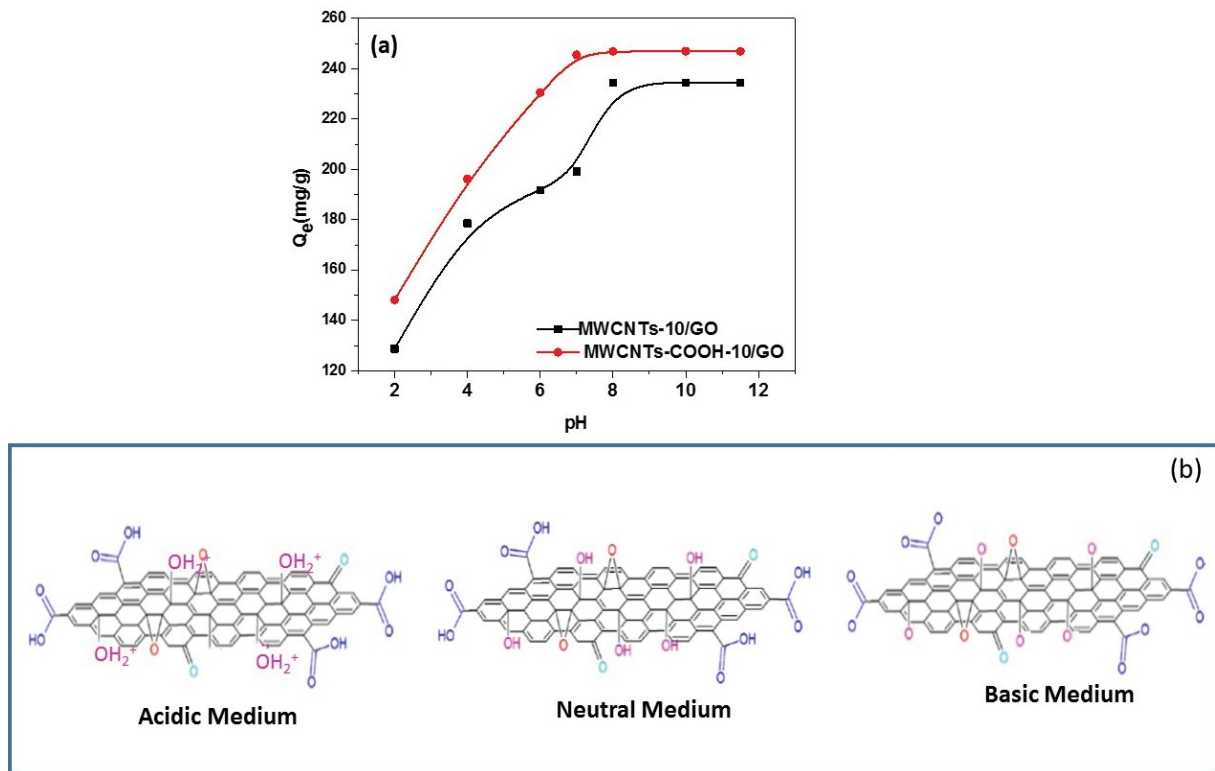
Fig. 6. (a) Influence of pH on the adsorption of methylene blue (MB) over MWCNTs-10/GO and MWCNTs-COOH-10/GO composite and (b) the surface charge of GO in a different medium.
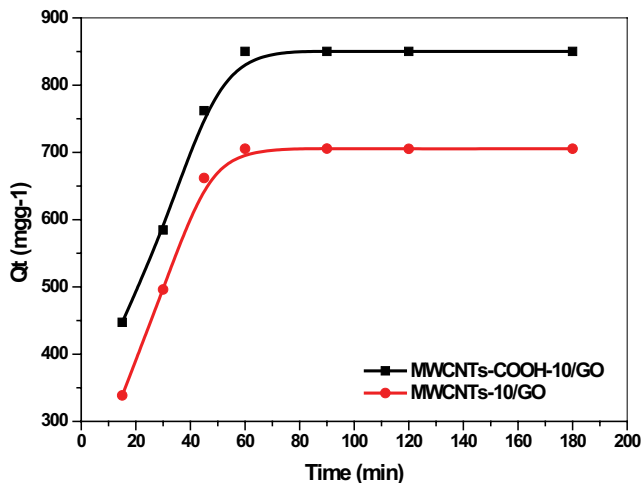


Fig. 7. Impact of the adsorption time on the adsorption of methylene blue (MB) over MWCNTs-10/GO and MWCNTs-COOH-10/GO composite.

various quantities from 10 to 60 mg. Fig. 8 shows that the removal raised with increasing the adsorbent dosage from 10 to 60 mg due to the high surface area; that is, leading to increase the opportunity of more removal sites [49]. In addition, the removal capacity was declined with increasing the sorbent dosage. At high dosage the accessible MB molecules were not enough to meet all the active centers; in other words, at large dose adsorbed, the adsorption centers could not reach equilibrium.

The adsorption kinetics assessment was carried out to emphasize the effect of adsorption time on the removal of MB onto MWCNTs-10/GO and MWCNTs-COOH-10/GO at pH 8.5. To acquire the pertinent kinetics variables, which were estimated by applying the pseudo-first-order (Eq. (4)), pseudo-second-order (Eq. (5)) and Elovich (Eq. (6)) kinetic models.

$$\log\left(Q_e - Q_t\right) = \log Q_e - \frac{k_1 t}{2.303} \tag{4}$$

$$\frac{t}{Q_t} = \frac{1}{k_2 Q_e^2} + \frac{1}{Q_e}t \tag{5}$$

$$Q_t = \frac{1}{\beta}\ln\left(\alpha\beta\right) + \frac{1}{\beta}\ln\left(t\right) \tag{6}$$

where $k_1$ (min$^{-1}$) and $k_2$ (g mg$^{-1}$ min$^{-1}$) are the pseudo-first-order and pseudo-second-order rate constants, respectively. $Q_e$ and $Q_t$ (mg g$^{-1}$) are the same mentioned above in the experimental section. The constants $\alpha$ and $\beta$ can be estimated from the slope and intercept of the Temkin plot. Linear relation of $\log\left(Q_e - Q_t\right)$ vs. $t$, $t/Q_t$ vs. $t$ and $Q_t$ vs. $\ln t$, are depicted for various kinetics models (Fig. 9 and Table 2). The regression factor $r^2$ of the pseudo-second-order model was 0.988 and 0.992 for both MWCNTs-10/GO and MWCNTs-COOH-10/GO, respectively, while the calculated adsorption capacities ($Q_e$) were 761.01 and 925.9 mg g$^{-1}$, in accordance with the obtained measured capacity of 705.4 and 850.1 mg g$^{-1}$,
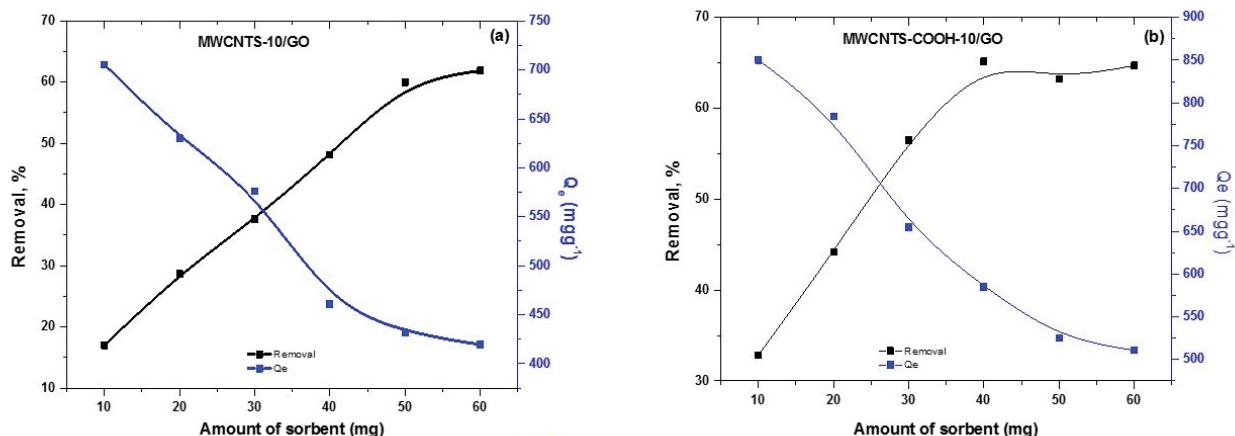
Fig. 8. Influence of the composite dose on the adsorption of methylene blue (MB) over (a) MWCNTs-10/GO and (b) MWCNTs-COOH-10/GO composite.
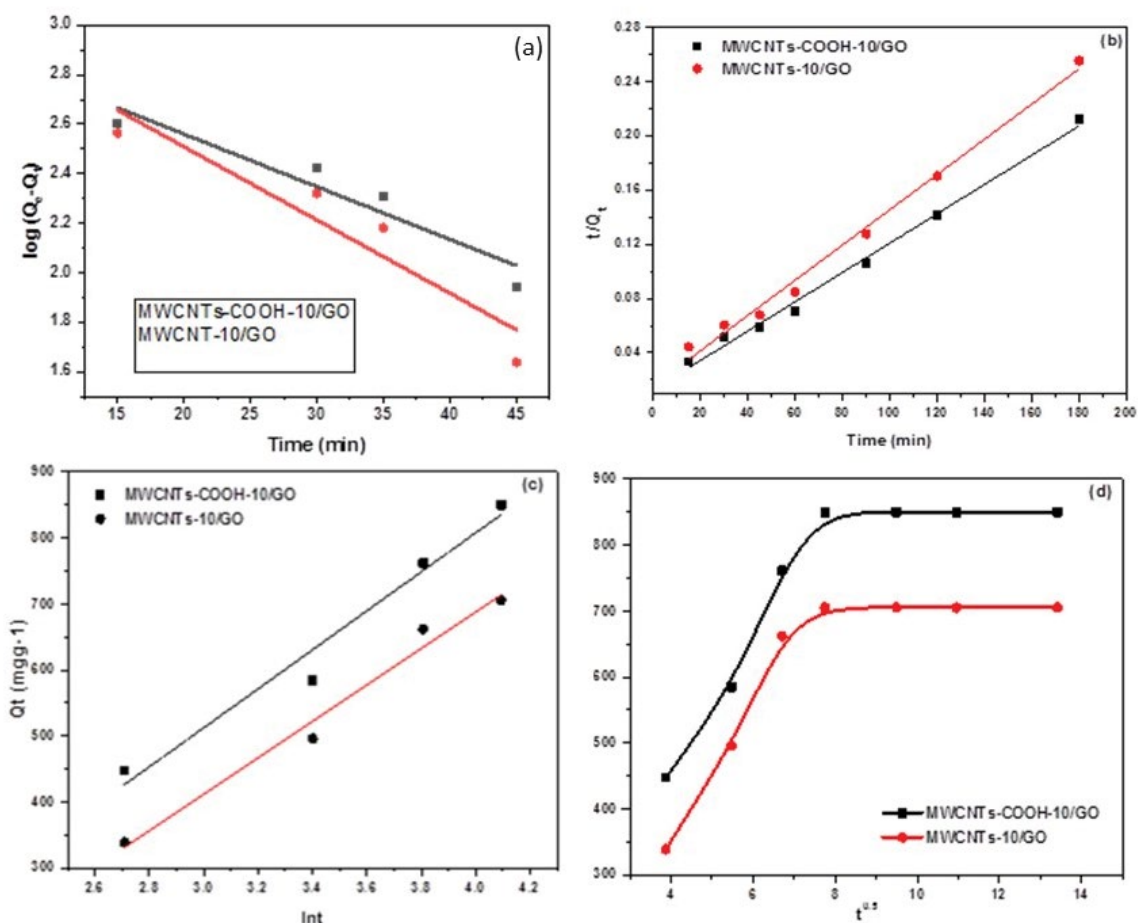


Fig. 9. Pseudo-first-order (a), Pseudo-second-order (b), Elovich (c), and intraparticle diffusion model (d) for the adsorption of methylene blue over MWCNTs-10/GO and MWCNTs-COOH-10/GO composites.

respectively. These data indicated that the adsorption of MB onto MWCNTs-10/GO and MWCNTs-COOH-10/GO could be well-featured by the pseudo-second-order kinetics model [49]. The pseudo-second-order and Elovich kinetic models were not fitting the experimental data. The kinetic data were fitted to the intraparticle diffusion to achieve more perspective into the adsorption mechanism. The intra-particle diffusion model was determined by Eq. (7):

$$Q_e = K_{id}t^{0.5} + C \tag{7}$$

Table 2
First-order, second-order, Elovich and intraparticle diffusion model constants, and their respective coefficients for the adsorption of MB onto MWCNTs-10/GO and MWCNTs-COOH-10/GO composite

| Parameters | Composite | |
|---|---|---|
| | MWCNTs-10/GO | MWCNTs-COOH-10/GO |
| Pseudo-first-order | | |
| $r^2$ | 0.862 | 0.834 |
| $k_1$ (min$^{-1}$) | 0.055 | 0.144 |
| $Q_e$ (mg g$^{-1}$) | 945.99 | 1,258.92 |
| Experimental $q_e$ (mg g$^{-1}$) | 705.4 | 850.1 |
| Pseudo-second-order | | |
| $r^2$ | 0.988 | 0.992 |
| $k_2$ (g mg$^{-1}$ min$^{-1}$) | $8.89 \times 10^{-5}$ | $1.14 \times 10^{-4}$ |
| $Q_e$ (mgg$^{-1}$) | 761.01 | 925.9 |
| Elovich model | | |
| $r^2$ | 0.972 | 0.955 |
| $\alpha$ | 61.05 | 83.77 |
| $\beta$ | $3.62 \times 10^{-3}$ | $3.39 \times 10^{-3}$ |
| Intraparticle diffusion | | |
| $r^2$ | 0.541 | 0.607 |
| $K_{int}$ (mg g$^{-1}$ min$^{-1/2}$) | 34.52 | 40.39 |
| $C_i$ (ppm) | 332.53 | 409.31 |

where $K_{id}$ (mg g$^{-1}$ min$^{-1/2}$) is the intraparticle diffusion rate constants. The results revealed that the adsorption of MB onto MWCNTs-10/GO and MWCNTs-COOH-10/GO was monitored by two distinct steps. Furthermore, the plots did not pass through the origin indicating that the intraparticle diffusion was not just a rate-controlling step and the boundary diffusion layer also affected the removal process [49].

### 3.2.5. Influence of concentration and adsorption isotherms of MB dye

The equilibrium isotherms for the removal of MB onto MWCNTs-10/GO and MWCNTs-COOH-10/GO at three various temperatures (298, 303 and 318 K) are depicted in Figs. 10a and b. The adsorption capacity was decreased with temperature raising from 298 to 318 K indicating exothermic kind of the adsorption process. The adsorption isotherms describe how MB dye molecules distribute between the liquid and solid adsorbent at equilibrium in the adsorption process. The treatment of the isotherm data by matching them with various isothermic models is a crucial point in finding the appropriate model for modeling objectives [50]. The experimental isotherm data were fitted to Freundlich (Eq. (8)), Langmuir (Eq. (9)) and Temkin (Eq. (10)) isotherm models.

$$\frac{C_e}{Q_e} = \frac{1}{Q_{\max}} C_e + \frac{1}{Q_{\max}} K_L \qquad (8)$$

$$\log Q_e = \log K_f + \frac{1}{n} \log C_e \qquad (9)$$

$$Q_e = B \ln A_T + \frac{RT}{b_T} \ln C_e \qquad (10)$$

where $Q_e$ and $C_e$ are the quantity of MB adsorbed at equilibrium (mg g$^{-1}$) and $C_e$ is the equilibrium concentration (mg L$^{-1}$). $K_f$ (mg g$^{-1}$) and $n$ are Freundlich constants, which assigned to the adsorption capacity and adsorption intensity, respectively. $Q_m$ is the maximum quantity of adsorption (mg g$^{-1}$), and $K_L$ is Langmuir constant related to the adsorption energy (L mg$^{-1}$). $A_T$ = the equilibrium binding constant, (L g$^{-1}$), $b_T$ = the adsorption constant (J mol$^{-1}$ K$^{-1}$), $R$ = ideal gas constant (8.314 J mol$^{-1}$ K$^{-1}$), $T$ = absolute temperature value (298, 303, and 318 K), $B$ = a constant related to the heat of sorption (J mol$^{-1}$).

As displayed in Fig. 11 and Table 3, the adsorption data of MB on MWCNTs-10/GO and MWCNTs-COOH-10/GO were fitting well with Langmuir isotherm, with the highest correlation factor for both sorbents at studied temperatures. In contrast, the low correlation factor ($r^2$) of Freundlich and Temkin isotherms indicated that they do not obey both isotherms (Figs. S1 and S2). Finally, the correlation factor ($r^2$) of various isotherms allows the experimental data fitting to rank as Langmuir > Freundlich > Temkin. These observations indicate that the coupling of functionalized MWCNTS with GO favors the adsorption capacity of MB in a monolayer coverage [49,51,52]. Hence, it is beneficial
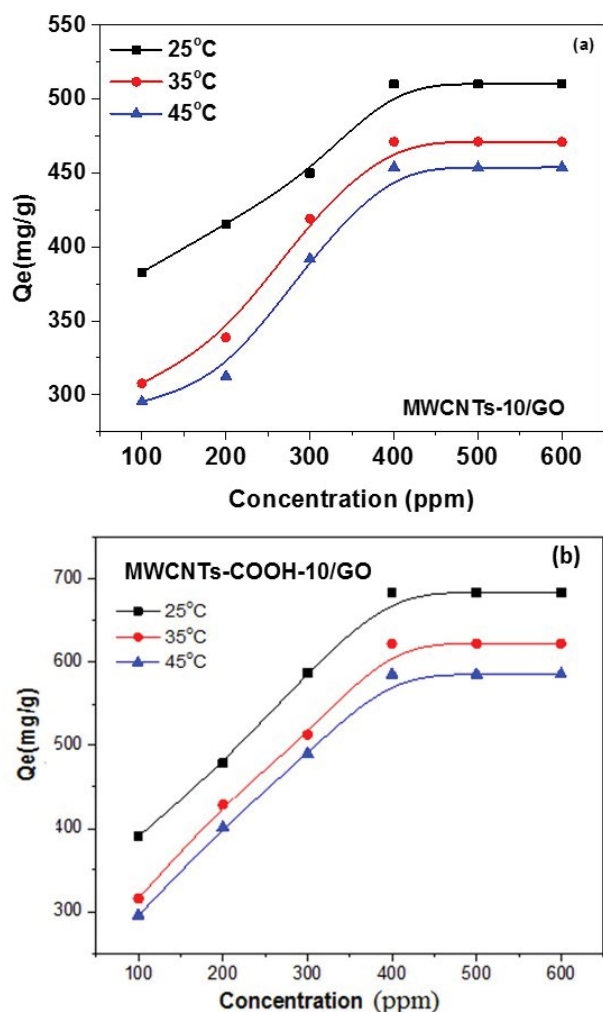
Fig. 10. Influence of initial concentration of MB adsorbed over (a) MWCNTs-10/GO and (b) MWCNTs-COOH-10/GO composite.

to apply MWCNTs-COOH-10/GO as adsorbents with the remarkable 3D nanotubular structure for the cleaning process.

### 3.2.6. Temperature effect and thermodynamic studies

The effect of temperature on the removal of MB dye was examined under isothermal conditions at the temperature 298, 303, and 318 K. As shown in Fig. 10, the adsorption capacities for MWCNTs-COOH-10/GO and MWCNTs-10/GO was decreased with increasing the temperature. The Thermodynamic functions can be estimated from the thermodynamic equilibrium constant, $K_0$. The change in free energy ($\Delta G°$), enthalpy ($\Delta H°$), and entropy ($\Delta S°$) were estimated by applying Eqs. (11)–(13):

$$\Delta G° = -RT \ln K_0 \tag{11}$$

$$K_0 = \frac{C_{ads}}{C_e} \tag{12}$$

$$\ln K_0 = \frac{\Delta S°}{R} - \frac{\Delta H°}{RT} \tag{13}$$

$K_0$ can be defined by Eq. (14) [53]:

$$K_0 = \frac{a_s}{a_e} = \left(\frac{\gamma_{ads}}{\gamma_e}\right)\left(\frac{C_s}{C_e}\right) \tag{14}$$

where $a_s$ is the activity of adsorbed MB, $a_e$ is the activity of MB in solution at equilibrium. $\gamma_{ads}$ is the activity coefficient of adsorbed MB, while $\gamma_e$ is the activity coefficient of MB in equilibrium solution. $C_{ads}$ are the MB adsorbed onto sorbents and $C_e$ is the concentration of MB at equilibrium. $K_0$ is simplified by suggesting that the concentration in the solution approaches zero for limiting cases corresponding to $C_{ads} \to 0$
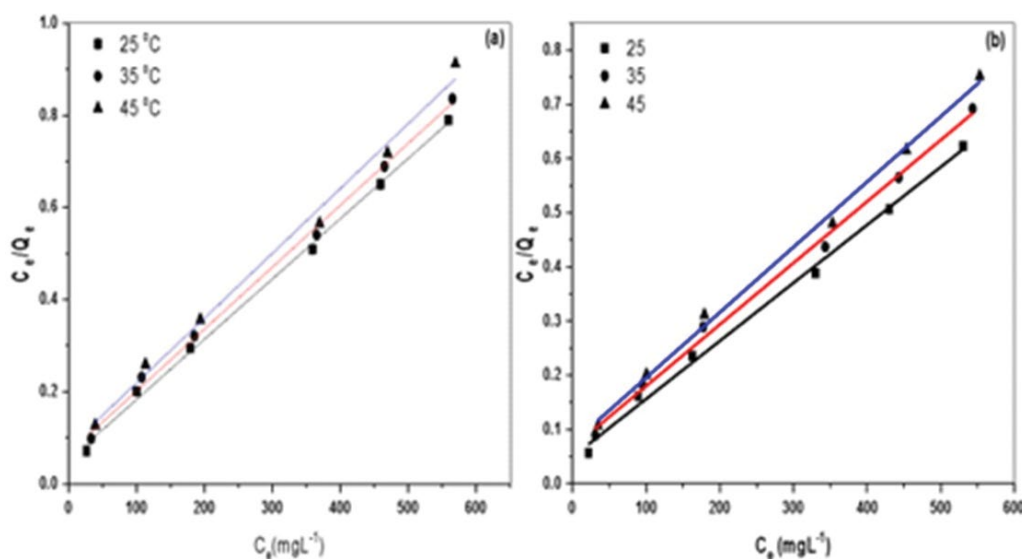


Fig. 11. Langmuir isotherms for adsorption of methylene blue over (a) MWCNTs-10/GO and (b) MWCNTs-COOH-10/GO composites.

Table 3
Adsorption isotherm models and their respective parameters for the adsorption of MB onto MWCNTs-10/GO and MWCNTs-COOH-10/GO composites

| Models | Adsorbents | | | | | |
|---|---|---|---|---|---|---|
| | MWCNTs-COOH-10/GO | | | MWCNTs-10/GO | | |
| | Temperature/°C | | | Temperature/°C | | |
| | 25°C | 35°C | 45°C | 25°C | 35°C | 45°C |
| Langmuir | | | | | | |
| $Q_{max}$ (mg g$^{-1}$) | 934.58 | 877.19 | 826.45 | 769.22 | 752.61 | 740.70 |
| $K_L$ | $2.3 \times 10^{-5}$ | $1.9 \times 10^{-5}$ | $7.01 \times 10^{-3}$ | $1.9 \times 10^{-5}$ | $6.06 \times 10^{-3}$ | $4.76 \times 10^{-3}$ |
| $r^2$ | 0.995 | 0.995 | 0.996 | 0.997 | 0.996 | 0.993 |
| Freundlich | | | | | | |
| $K_f$ (mg g$^{-1}$) | 154.88 | 109.64 | 91.20 | 272.9 | 151.3 | 138.9 |
| $n$ | 3.47 | 3.98 | 2.78 | 3.99 | 3.39 | 2.92 |
| $r^2$ | 0.992 | 0.994 | 0.990 | 0. 993 | 0.991 | 0.995 |
| Temkin | | | | | | |
| $b_T$ (J mol$^{-1}$ K$^{-1}$) | 103.1 | 118.2 | 130.2 | 41.5 | 69.9 | 68.4 |
| $A_T$ (L g$^{-1}$) | 50.1 | −101.9 | −199.4 | 240.2 | 35.8 | 20.7 |
| $r^2$ | 0.887 | 0.945 | 0.975 | 0.789 | 0.817 | 0.729 |

and $C_e \rightarrow 0$. The ratio of all activity coefficients close unity for small concentrations (Eq. (15)) [53]:

$$C_s \lim \rightarrow 0 = \frac{C_{ads}}{C_e} = \frac{a_{ads}}{a_e} = K_0 \qquad (15)$$

$K_0$ (at different temperatures) was determined by plotting $\ln(C_{ads}/C_e)$ vs. $C_{ads}$ and extrapolating $C_{ads}$ to zero [53,54]. $K_0$ values were decreased with rising temperature, and the adsorption is considered to be exothermic (Table 4). $\Delta G°$ indicated spontaneous uptake and the process spontaneity is raised with increasing temperature. The values of $\Delta H°$ and $\Delta S°$ were estimated from the linear plot of $\ln K_0$ vs. $1/T$ from the slope and intercept, respectively (Fig. S3). The enthalpy change ($\Delta H°$ is negative) suggested that the MB adsorption onto MWCNTs-COOH-10/GO and MWCNTs-10/GO sorbents is exothermic [53]. The negative entropy change ($\Delta S°$) displayed the affinity between MB and adsorbent.

### 3.3. Reusability of MWCNTs-10/GO and MWCNTs-COOH-10/GO for MB removal

Adsorption/desorption investigations were carried out using a mixture of 0.1 of HCl and 0.1 mol L$^{-1}$ NaCl as eluent owing to examine the possibility of reactivation and reusability of MWCNTs-10/GO and MWCNTs-COOH-10/GO sorbents. Their reusability was examined four times (Figs. 12a and b). The desorption was found to be higher than 80% over four cycles with ~90% adsorption. Therefore, it can be concluded that the MWCNTs-10/GO and MWCNTs-COOH-10/GO with great stability could be used as excellent reusable sorbents for MB removal.

### 3.4. Application

To evaluate the practical applications in the large-scale industry, the adsorption performance of MWCNTs-10/GO and MWCNTs-COOH-10/GO was tested using various water samples as DIW, Tap water, and Seawater. A solution

Table 4
Thermodynamic parameters for the adsorption of MB onto MWCNTs-10/GO and MWCNTs-COOH-10/GO composite

| Temperature, K | Adsorbents | | | | | |
|---|---|---|---|---|---|---|
| | MWCNTs-10/GO | | | MWCNTs-COOH-10/GO | | |
| | Thermodynamic parameters | | | | | |
| | $\Delta H$ (kJ mol$^{-1}$) | $\Delta G$ (kJ mol$^{-1}$) | $\Delta S$ (kJ mol$^{-1}$) | $\Delta H$ (kJ mol$^{-1}$) | $\Delta G$ (kJ mol$^{-1}$) | $\Delta S$ (kJ mol$^{-1}$) |
| 298 | | −45.4 | | | −29.6 | |
| 308 | −5.10 | −1.34 | −2.56 | −3.26 | −0.87 | −1.59 |
| 318 | | −2.96 | | | −2.73 | |
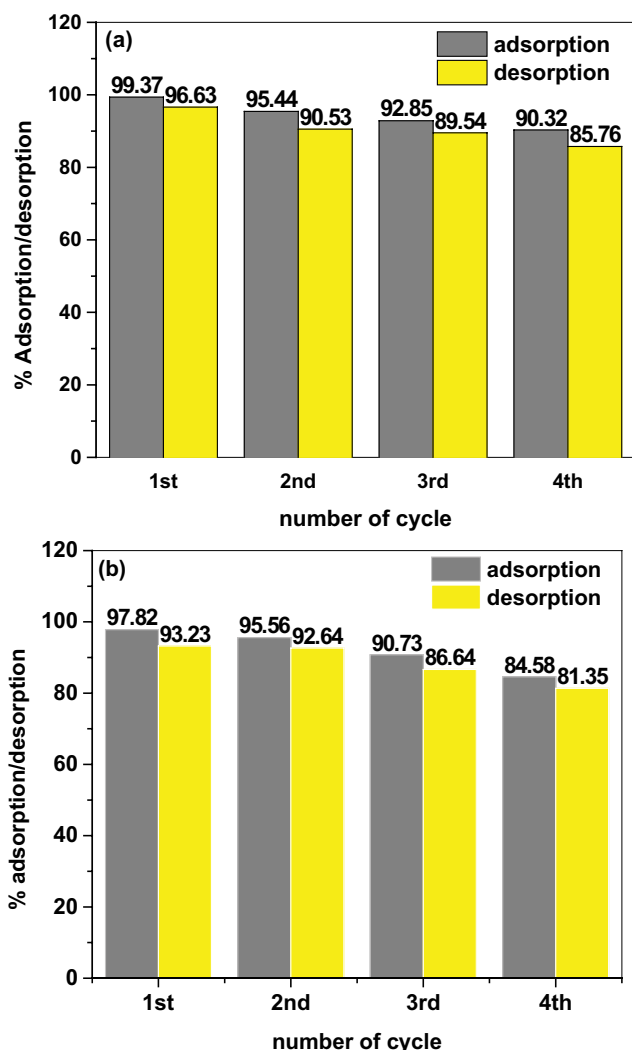
Fig. 12. Elution/reuses assessment over (a) MWCNTs-COOH-10/GO and (b) MWCNTs-10/GO composites.
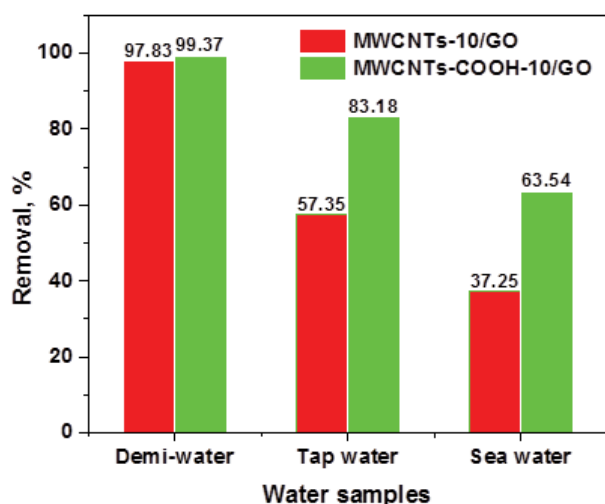


Fig. 13. Methylene blue removal using (a) MWCNTs-10/GO and (b) MWCNTs-COOH-10/GO composite in various water samples.

Table 5
Comparison of adsorption capacity of various adsorbents for MB dye removal

| Adsorbent | Adsorption capacity, mg g$^{-1}$ | Reference |
|---|---|---|
| Bamboo-based active carbon | 454.2 | [14] |
| Activated clay | 50.22 | [16] |
| Carbon nanotube | 46.2 | [18] |
| GO | 714 | [26] |
| Porous regenerated cellulose | 144.09 | [53] |
| MWCNTs-COOH-10/GO | 850.1 | Present study |
| MWCNTs-10/GO | 705.4 | Present study |

of MB in a different water sample (50 mg L$^{-1}$) was used for all experiments at optimum parameters. Fig. 13 illustrates the removal efficacy of MB in different water samples containing various foreign ions. The removal efficacy of MB in different water sources was found to be ranked as DIW > Tap water > Seawater. These results confirm that the removal efficacy of MB considerably influenced by the ordinary existing ions in the water samples.

### 3.5. Comparison study

Table 5 shows the comparison of the proposed composites MWCNTs-COOH-10/GO and MWCNTs-10/GO results with number of absorbents notified in literature for the uptake of MB with, it is clear that the adsorption ability of our composites exhibits high removal efficiency compared to the previous works.

### 4. Conclusion

In conclusion, the present study is dealing with the ability to adsorb MB dye onto novel 3D- carbon architecture composites (MWCNTs-10/GO and MWCNTs-COOH-10/GO). The optimal parameters (pH, contact time, a dose of composite and concentration of dye at different temperatures) were performed to optimize the removal process. The removal processes were matched with Langmuir isotherm and follow the pseudo-second-order kinetic model. The thermodynamic functions ($-\Delta G°$, $-\Delta H°$ and $-\Delta S°$) exhibit spontaneous, exothermic and more ordered at the interface between MB and adsorbent, respectively, adsorption processes. The sorbents attained a great degree of regeneration and the material conserved its original structure and removal activity after being regenerated four times.

### References

[1] K.M. Parida, S. Sahu, K.H. Reddy, P.C. Sahoo, A kinetic, thermodynamic, and mechanistic approach toward adsorption of methylene blue over water-washed manganese nodule leached residues, Ind. Eng. Chem. Res., 50 (2011) 843–848.
[2] Z. Aksu, Application of biosorption for the removal of organic pollutants: a review, Process Biochem., 40 (2005) 997–1026.
[3] S.C.R. Santos, R.A.R. Boaventura, Adsorption modeling of textile dyes by sepiolite, Appl. Clay Sci., 42 (2008) 137–145.
[4] Y. Li, Q. Du, T. Liu, X. Peng, J. Wang, J. Sun, Y. Wang, S. Wu, Z. Wang, Y. Xia, L. Xia, Comparative study of methylene blue

dye adsorption onto activated carbon, graphene oxide, and carbon nanotubes, Chem. Eng. Res. Des., 91 (2013) 361–368.

[5] Y. Li, Q. Du, T. Liu, Y. Qi, P. Zhang, Z. Wang, Y. Xia, Preparation of activated carbon from *Enteromorpha prolifera* and its use on cationic red X-GRL removal, Appl. Surf. Sci., 257 (2011) 10621–10627.

[6] B. Coasne, C. Alba-Simionesco, F. Audonnet, G. Dosseh, K.E. Gubbins., Adsorption, structure and dynamics of benzene in ordered and disordered porous carbons, Phys. Chem. Chem. Phys., 13 (2011) 3748–3757.

[7] Q. Du, J. Sun, Y. Li, X. Yang, X. Wang, Z. Wang, L. Xia., Highly enhanced adsorption of Congo red onto graphene oxide/ chitosan fibers by wet-chemical etching off silica nanoparticles, Chem. Eng. J., 245 (2014) 99–106.

[8] M. Sadrnourmohamadi, B. Gorczyca, Removal of dissolved organic carbon (DOC) from high DOC and hardness water by chemical coagulation: relative importance of monomeric, polymeric, and colloidal aluminum species, Sep. Sci. Technol., 50 (2015) 2075–2085.

[9] R.V. Kumar, A.K. Ghoshal, G. Pugazhenthi, Fabrication of zirconia composite membrane by in situ hydrothermal technique and its application in separation of methyl orange, Ecotoxicol. Environ. Saf., 121 (2015) 73–79.

[10] A. Kar, Y.R. Smith, V. Subramanian, Improved photocatalytic degradation of textile dye using titanium dioxide nanotubes formed over titanium wires. Environ. Sci. Technol., 43 (2009) 3260–3265.

[11] F. Gulshan, S. Yanagida, Y. Kameshima, Various factors affecting photodecomposition of methylene blue by iron-oxides in an oxalate solution, Water Res., 44 (2010) 2876–2884.

[12] M.H. El-Naas, S.A. Al-Muhtaseb, S. Makhlouf, Biodegradation of phenol by pseudomonas putida immobilized in polyvinyl alcohol (PVA) gel, J. Hazard. Mater., 164 (2009) 720–725.

[13] Y.H. Li, P. Zhang, Q. Du, X. Peng, T. Liu, Z. Wang, Adsorption of fluoride from aqueous solution by graphene, J. Colloid Interface Sci., 363 (2013) 348–354.

[14] B.H. Hameed, A.T.M. Din, A.L. Ahmad, Adsorption of methylene blue onto bamboo-based activated carbon: kinetics and equilibrium studies, J. Hazard. Mater., 141 (2007) 819–825.

[15] D. Kavitha, C. Namasivayam, Experimental and kinetic studies on methylene blue adsorption by coir pith carbon, Bioresour. Technol., 98 (2007) 14–21.

[16] K. Allam, K. Gourai, A. EL Bouari, B. Belhorma, L. Bih, Adsorption of Methylene Blue on raw and activated clay: case study of Bengurir clay, J. Mater. Environ. Sci., 9 (2018) 1750–1761.

[17] B. Bestani, N. Benderdouche, B. Benstaali, M. Belhakem, A. Addou, Methylene blue and iodine adsorption onto an activated desert plant, Bioresour. Technol., 99 (2008) 8441–8444.

[18] Y. Yao, F. Xu, M. Chen, Z. Xu, Z. Zhu, Adsorption behavior of methylene blue on carbon nanotubes, Bioresour. Technol., 101 (2010) 3040–3046.

[19] T. Liu, Y.H. Li, Q.J. Du, Adsorption of methylene blue from aqueous solution by graphene, Colloids Surf., B, 90 (2012)197–203.

[20] Y.Y. Liang, D.Q. Wu, X.L. Feng, Dispersion of graphene sheets in organic solvent supported by ionic interactions, Adv. Mater., 21 (2009) 1679–1683.

[21] Q. Su, S.P. Pang, V. Alijani, Composites of graphene with large aromatic molecules, Adv. Mater., 21 (2009) 3191–3195.

[22] S. Park, R.S. Ruoff, Chemical methods for the production of graphenes, Nat. Nanotechnol., 4 (2009) 217–224.

[23] D.R. Dreyer, S. Park, C.W. Bielawski, R.S. Ruoff, The chemistry of graphene oxide, Chem. Soc. Rev., 39 (2010) 228–240.

[24] S.I. El-Hout, H. Suzuki, S.M. El-Sheikh, H.M.A. Hassan, F.A. Harraz, I.A. Ibrahim, E.A. El-Sharkawy, S. Tsujimura, M. Holzinger, Y. Nishina, Tuning the redox potential of vitamin K3 derivatives by oxidative functionalization using a Ag(I)/GO catalyst, Chem. Commun., 53 (2018) 8890–8893.

[25] S.I. El-Hout, S.M. El-Sheikh, H.M.A. Hassan, F.A. Harraz, I.A. Ibrahim, E.A. El-Sharkawy, A green chemical route for synthesis of graphene supported palladium nanoparticles:

[26] a highly active and recyclable catalyst for reduction of nitrobenzene, Appl. Catal., A, 503 (2015) 176–185.

[26] S.-T. Yang, S. Chen, Y. Chang, A. Cao, Y. Liu, H. Wang, Removal of methylene blue from aqueous solution by graphene oxide, J. Colloid Interface Sci., 359 (2011) 24–29.

[27] S. Beg, M. Rizwan, A.M. Sheikh, M.S. Hasnain, K. Anwer, K. Kohli, Advancement in carbon nanotubes: basics, biomedical applications and toxicity, J. Pharm. Pharm., 63 (2011) 141–163.

[28] Z.F. Liu, L.Y. Jiao, Y.G. Yao, X.J. Xian, J. Zhang, Aligned, ultralong single-walled carbon nanotubes: from synthesis, sorting, to electronic devices, Adv. Mater., 22 (2010) 2285–2310.

[29] Y. Rosen, N.M. Elman, Carbon nanotubes in drug delivery: focus on infectious diseases, Expert Opin. Drug Delivery, 6 (2009) 517–530.

[30] D. Robati, B. Mirza, R. Ghazisaeidi, M. Rajabi, O. Moradi, I. Tyagi, S. Agarwal, V.K. Gupta, Adsorption behavior of methylene blue dye on nanocomposite multi-walled carbon nanotube functionalized thiol (MWCNT-SH) as new adsorbent, J. Mol. Liq., 216 (2016) 830–835.

[31] N.G. Sahoo, S. Rana, J.W. Cho, L. Li, S.H. Chan, Polymer nanocomposites based on functionalized carbon nanotubes, Prog. Polym. Sci., 35 (2010) 837–867.

[32] V. Datsyuk, M. Kalyva, K. Papagelis, J. Parthenios, D. Tasis, Chemical oxidation of multiwalled carbon nanotubes, Carbon, 46 (2008) 833–840.

[33] Z. Wang, M.D. Shirley, S.T. Meikle, R.L.D. Whitby, The surface acidity of acid oxidized multi-walled carbon nanotubes and the influence of in-situ generated fulvic acids on their stability in aqueous dispersions, Carbon, 47 (2009) 73–79.

[34] J.L. Vicente, A. Albesa, J.L. Lianos, E.S. Flores, A.E. Fertitta, Effect of acid oxidation treatment on adsorption properties of arc-discharge synthesized multiwall carbon nanotubes, J. Argent. Chem. Soc., 98 (2011) 29–38.

[35] L. Fan, C. Luo, M. Sun, X. Li, F. Lu, H. Qiu, Preparation of novel magnetic chitosan/graphene oxide composite as effective adsorbents toward methylene blue, Bioresour. Technol., 114 (2012) 703–706.

[36] N.A. Travlou, G.Z. Kyzas, N.K. Lazaridis, E.A. Deliyanni, Graphite oxide/chitosan composite for reactive dye removal, Chem. Eng. J., 217 (2013) 256–265.

[37] H. Shi, L. Weisong, L. Zhong, C Xu, Methylene blue adsorption from aqueous solution by magnetic cellulose/graphene oxide composite: equilibrium, kinetics, and thermodynamics, Ind. Eng. Chem. Res., 53 (2014) 1108–1118.

[38] M.Z. Siregar, A.H. Ritonga, Multi-walled carbon nanotubes/ chitosan nanocomposite from oil palm shell as adsorbent to reduce levels of metal Hg ion in liquid waste gold mine, Int. J. Adv. Res. Chem. Sci., 3 (2016) 40–46.

[39] W.S. Hummers, R.E. Offeman, Preparation of graphitic oxide, J. Am. Chem. Soc., 80 (1958) 1339.

[40] H.M.A. Hassan, V. Abdelsayed, A.S. Khder, K.M. Abou Zeid, J. Terner, M.S. El-Shall, S.I. Al-Resayes, A.A. El-Azhary, Microwave synthesis of graphene sheets supporting metal nanocrystals in aqueous and organic media, J. Mater. Chem., 19 (2009) 3832–3837.

[41] M.S. Tehrani1, P.A. Azar, P.E. Namin, S.M. Dehaghi, Removal of lead ions from wastewater using functionalized multuwalled carbon nanotubes with tris(2-aminoethyl) amine, J. Environ. Prot., 4 (2013) 529–536.

[42] D. Zhang, T. Yan, L. Shi, Z. Peng, X. Wen, J. Zhang, Enhanced capacitive deionization performance of grapheme/carbon nanotube composites, J. Mater. Chem., 22 (2012) 14696.

[43] K.B. Vijayan, N.M. Dimitrijevic, D. Finkelstein-Shapiro, J. Wu, K.A. Gray, Coupling titania nanotubes and carbon nanotubes to create photocatalytic nanocomposites, ACS Catal., 2 (2012) 223–229.

[44] D. Konios, M.M. Stylianakis, E. Stratakis, E. Kymakis, Dispersion behaviour of graphene oxide and reduced graphene oxide, J. Colloid Interface Sci., 430 (2014) 108–112.

[45] M.B. Swami, A.H. Jadhav, S.R. Mathpati, H.G. Ghuge, S.G. Patil, Eco-friendly highly efficient solvent free synthesis of benzimidazole derivatives over sulfonic acid functionalized

graphene oxide in ambient condition, Res. Chem. Intermed., 43 (2017) 2033–2053.

[46] M. Kelen, N. Sanli, Determination of pK$_a$ of some auxins in methanol – water mixtures by reversed phase liquid chromatography and potentiometric methods, J. Braz. Chem. Soc., 20 (2009) 133–140.

[47] R. Andonouski, L. Spirevska, A. Nikolovski, UV study of protonation of indole and 3- substituted indols in perchloric acid media, Croat. Chem. Acta., 69 (1996) 1201–1213.

[48] S.G. Aziz, A.O. Aloubi, S.A. Elrobi, R.H. Hilal, Electronic structure and acid- base properties of kojic acid and its dimers. A DFT and quantum topology study, Mol. Phys., 115 (2017) 2565–2576.

[49] E.M. Saad, H.M.A. Hassan, M.S. Soltan, I.S. Butler, S.I. Mostafa, Removal of copper(II) ions from aqueous media by chemically modified MCM-41 with N-(3-(trimethoxysilyl)propyl) ethylenediamine and its 4-hydroxysalicylidene schiff-base, Environ. Prog. Sustainable Energy, 37 (2018) 746–760.

[50] Y. Li, J. Sun, Q. Du, L. Zhang, X. Yang, S. Wu, Y. Xia, Z. Wang, L. Xia, A. Cao, Mechanical and dye adsorption properties of

graphene oxide/chitosan composite fibers prepared by wet spinning, Carbohydr. Polym., 102 (2014) 755–761.

[51] S.A. Elsayed, E.M. Saad, I.S. Butler, S.I. Mostafa, 2-hydroxynaphthaldehyde chitosan schiff-base; new complexes, biosorbent to remove cadmium(II) ions from aqueous media and aquatic ecotoxicity against green alga *Pseudokirchneriella subcapitata*, J. Environ. Chem. Eng., 6 (2018) 3451–3468.

[52] H.A. El-Azim, M.M. El-Sayed Seleman, E.M. Saad, Applicability of water-spray electric arc furnace steel slag for removal of Cd and Mn ions from aqueous solutions and industrial wastewaters, J. Environ. Chem. Eng., 7 (2019) 1–12.

[53] Z.C. Li, H.T. Fan, Y. Zhang, M.X. Chen, Z.Y. Yu, X.Q. Cao, T. Sun. Cd(II)-imprinted polymer sorbents prepared by combination of surface imprinting technique with hydrothermal assisted sol–gel process for selective removal of cadmium(II) from aqueous solution, Chem. Eng. J., 171 (2011) 703–710.

[54] W. Wang, Q. Bai, T. Liang, H. Bai, X. Liu, Two-sided surface oxidized cellulose membranes modified with PEI: preparation, characterization and application for dyes removal, Polymers, 9 (2017) 455.

## Supplementary information
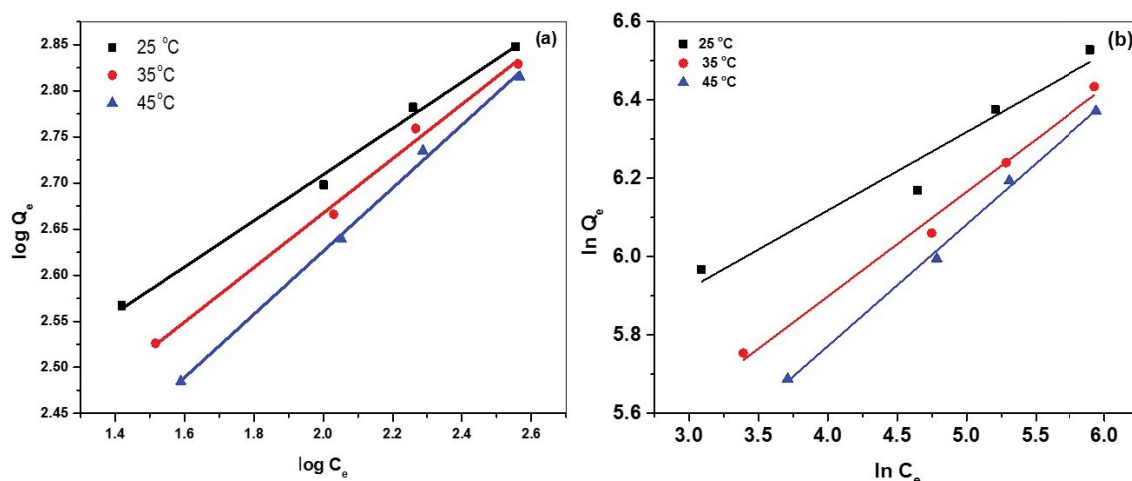


Fig. S1. Freundlich isotherms for adsorption of methylene blue over (a) MWCNTs-10/GO and (b) MWCNTs-COOH-10/GO composite.
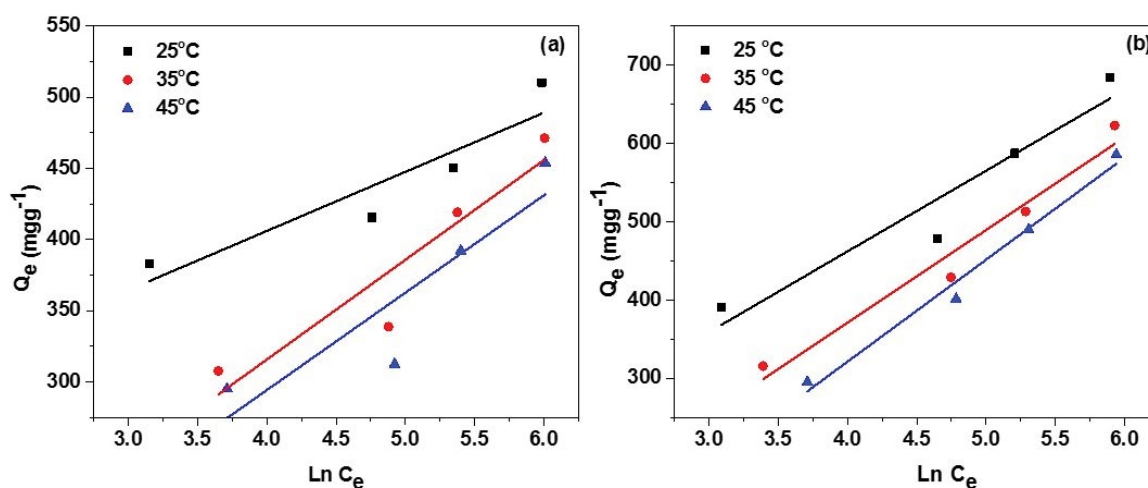


Fig. S2. Temkin isotherms for adsorption of methylene blue over (a) MWCNTs-10/GO and (b) MWCNTs-COOH-10/GO composite.
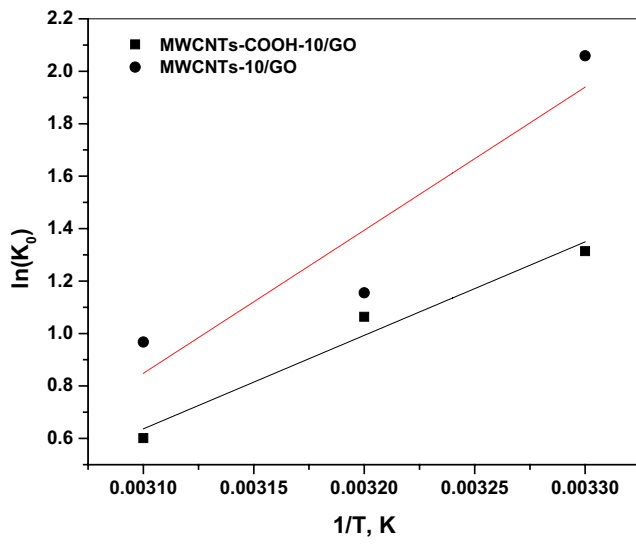
Fig. S3. Variation of equilibrium constant ($K_0$) as a function of temperature ($1/T$).